ELSEVIER

Journal of Structural Geology 30 (2008) 565–579

JOURNAL OF STRUCTURAL GEOLOGY

www.elsevier.com/locate/jsg

Dissolution-precipitation creep of K-feldspar in mid-crustal granite mylonites

Luca Menegon*, Giorgio Pennacchioni, Richard Spiess

Dipartimento di Geoscienze, Università degli Studi di Padova, via Giotto 1, 35137 Padova, Italy

Received 25 June 2007; received in revised form 14 January 2008; accepted 4 February 2008
Available online 13 February 2008

Abstract

The deformation of K-feldspar within lower amphibolite facies granite mylonites from the Gran Paradiso nappe (North-Western Alps, Italy) is primarily accomplished by dissolution, replacement and precipitation processes, with little or no evidence for dislocation glide or creep. New elongate grains of K-feldspar precipitate in dilational domains within and around K-feldspar porphyroclasts as a part of the process of myrmekite formation that progressively consumes the porphyroclasts. The new grains grow in epitaxial continuity with the parent porphyroclasts, which hinders the development of a bulk crystallographic preferred orientation (CPO) in the aggregates of new grains when large amounts of relict K-feldspar are still present. In mylonites, the magmatic K-feldspar is eventually transformed into 100–300 μm thick, nearly monomineralic, fine-grained (20–50 μm in size) aggregates of new grains showing an oblique shape fabric and a CPO. The observed CPO is not consistent with the activity of any slip system in K-feldspar. Instead, it is interpreted to result from dissolution-precipitation creep, with a slow reaction rate parallel to [010] and [001] crystallographic axes and a fast reaction rate parallel the [100] axis. Consistent with such a dissolution-precipitation mechanism, boundaries of new K-feldspar grains are highly corroded when oriented approximately parallel to the extensional instantaneous stretching axis, whereas boundaries approximately orthogonal to the same stretching axis show well-developed crystal facets. The CPO developed is weak, which suggests that the anisotropy in the dissolution/growth rate of K-feldspar is also weak.

Keywords: K-feldspar microstructure; Electron backscatter diffraction (EBSD); Crystallographic preferred orientation (CPO); Granite mylonite; Dissolution-precipitation creep; Deformation mechanisms

1. Introduction

K-feldspar is a major mineral component of many granitoids and its deformational behaviour is important for establishing the overall rheology of continental crust. Microstructure and crystallographic preferred orientation (CPO, texture) provide the link between natural and experimental examples of dynamically recrystallized aggregates and are thus powerful tools for the interpretation of rock rheology and for estimating different deformation parameters during ductile flow (e.g., Law, 1990; Passchier and Trouw, 1996). Although there are many detailed descriptions of microstructures of K-feldspar developed during deformation under a range of metamorphic conditions from greenschist to eclogite facies (e.g., Debat et al., 1978; Vidal et al., 1980; Simpson and Wintsch, 1989; Pryer, 1993; Altenberger and Wilhelm, 2000), only a few studies report the CPO of K-feldspar in dynamically recrystallized aggregates (Schulmann et al., 1996; Martelat et al., 1999; Franek et al., 2006; Ishii et al., 2007) or discuss the possible active slip systems (Tullis, 1983 and references therein).

The development of CPO in dynamically recrystallized aggregates within deformed rocks is commonly assumed to result by dislocation glide along specific slip systems, although the process of CPO development is not fully understood. Among the concurrent grain-scale processes that compete during recrystallization, dissolution-precipitation creep can be of primary importance in intergranular, fluid-assisted deformation. This mechanism, also referred to as 'stress-induced solution transfer' and/or 'pressure solution' (Vernon,

* Corresponding author. Tel.: +39 049 827 1863; fax: +39 049 827 2070.
E-mail address: luca.menegon@unipd.it (L. Menegon).

0191-8141/$ - see front matter © 2008 Elsevier Ltd. All rights reserved.
doi:10.1016/j.jsg.2008.02.001

2004), implies that grains are dissolved at sites of high normal stress, whereas new material, transported along intergranular fluid pathways, is added at sites of relatively low normal stress. Dissolution-precipitation creep can be efficient under low grade metamorphic conditions in fluid-rich environments (e.g., Hippertt, 1994a; Passchier and Trouw, 1996), but can also be important under amphibolite facies conditions (Berger and Stünitz, 1996; Wintsch and Yi, 2002) and during anatexis (Álvarez-Valero et al., 2005).

Whether dissolution-precipitation creep is capable of producing a CPO or not is still a matter of debate. That dissolution-precipitation creep can play a primary role in CPO development has been established, or at least proposed, for natural quartz deformed under low grade metamorphic conditions (Hippertt, 1994a; Stallard and Shelley, 1995; Takeshita and Hara, 1998), for experimentally deformed quartz (Vernooij et al., 2006), for naturally deformed clinopyroxene within eclogites (Godard and van Roermund, 1995) and for experimentally deformed albite (Heidelbach et al., 2000). Bons and den Brok (2000) also presented a numerical model in which dissolution-precipitation creep associated with rigid body rotation produced different CPOs that varied with the deformation regime.

In this paper we describe the deformation microstructures and CPO of K-feldspar within lower amphibolite facies granite mylonites of the Gran Paradiso nappe (NW Alps, Italy). The CPO data were measured by Electron Backscatter Diffraction (EBSD). Mylonitization occurred under water-rich conditions and was accompanied by grain-scale mass transfer, as shown by the characteristic synkinematic metamorphic reactions (e.g. myrmekite-forming reactions) and by the extensive development of microveins. The studied granite mylonites and the deformation conditions were similar to those described from the Ryoke metamorphic belt, NW Japan, by Ishii et al. (2007), although the metamorphic grade in their examples may be slightly lower (upper greenschist facies). Ishii et al. (2007) considered that the CPO of K-feldspar in the Ryoke granite mylonites was achieved by dislocation creep. Here we show that in the Gran Paradiso mylonites dissolution-precipitation creep was the dominant deformation mechanism of K-feldspar and played a major role in the development of the CPO.

2. Geological setting

The studied granite protomylonites and mylonites were sampled in the Penninic Gran Paradiso tectonic unit of the North-Western Alps (Italy). The Gran Paradiso unit is a slice of pre-Alpine mid-crustal continental rocks originally forming part of the paleo-European continental margin, which was involved in the polyphase Alpine orogeny (Dal Piaz et al., 1972). The pre-Alpine rocks of the Gran Paradiso nappe consist of amphibolite facies paragneisses and metabasites (Dal Piaz and Lombardo, 1986), which were intruded during the Permian by large, dominantly granitic intrusions (Ballèvre, 1988; Ring et al., 2005). The Alpine tectono-metamorphic evolution produced a pervasive reworking of the pre-Alpine protolith and involved an early high-pressure eclogitic stage followed by an upper greenschist to lower amphibolite facies stage during exhumation (Dal Piaz and Lombardo, 1986; Ballèvre, 1988; Borghi et al., 1996; Le Bayon et al., 2006). Granites were extensively converted to augen gneisses and mylonites, but massive- to weakly foliated metagranites are preserved in a kilometre-scale low-strain domain in the Piantonetto Valley (Callegari et al., 1969). Here the Alpine deformation is localized into different sets of discrete, lower amphibolite facies ductile shear zones (Menegon, 2006; Menegon et al., 2006) and it is the mylonites within these shear zones that are the subject of this paper (Figs. 1a,b).

3. The mylonitic shear zones of Piantonetto Valley

The granite protolith consists of K-feldspar (32% by volume), plagioclase (27%), quartz (27%), biotite (13%), and

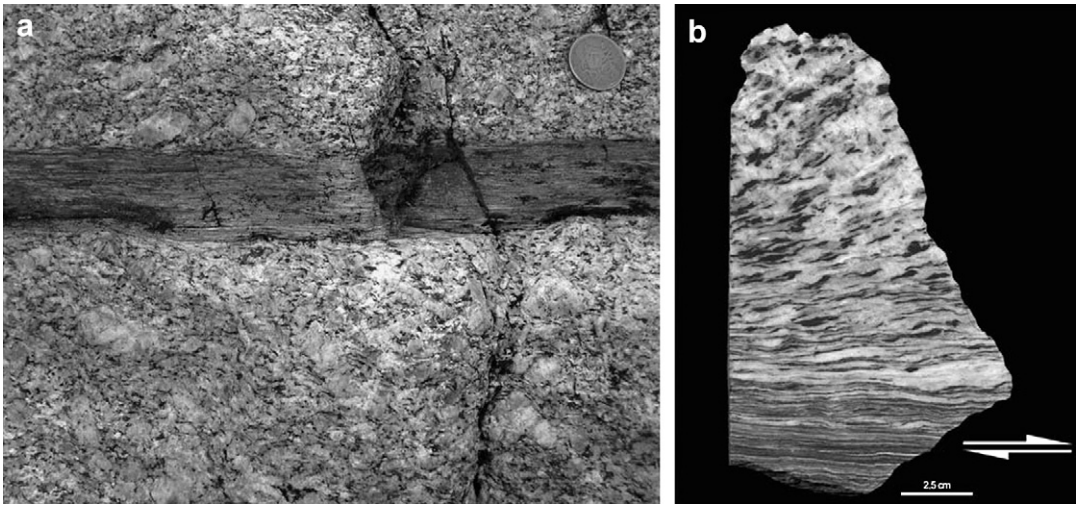

Fig. 1. (a) Localized ductile shear zone within metagranites of the Piantonetto Valley (Gran Paradiso nappe). UTM 32T 5037070 north, 371539 east; (b) The mylonite sample P15Z analysed in this study. UTM 32T 5038458 north, 372896 east. Sense of shear is dextral in both (a) and (b).

accessory apatite and zircon. The large (up to >1 cm in size) magmatic K-feldspar crystals have an equant to tabular shape and are often Carlsbad twinned.

Within the shear zones, the magmatic minerals are replaced by a synkinematic metamorphic assemblage including quartz, K-feldspar, plagioclase (An_{0-5} to An_{17-27}), biotite, white mica, epidote and titanite. In the weakly deformed granites, magmatic plagioclase is replaced by fine-grained plagioclase$_2$ + white mica + epidote ± garnet and magmatic biotite by biotite$_2$ ± white mica + titanite ± ilmenite (subscripts 1 and 2 refer to successive mineral generations and, in particular, to magmatic and metamorphic phases, respectively). These fine-grained replacement aggregates act as the stress-supporting matrix from the incipient stages of mylonitization and localize the deformation. Large K-feldspar crystals are dismembered by microfracturing and shearing along fine-grained aggregates derived by recrystallization of perthites and myrmekites (Menegon et al., 2006), but small K-feldspar porphyroclasts survive up to high strain.

The mylonites display a compositional layering defined by the alternation of polymineralic feldspar-rich layers (matrix grain size ≤50 μm), biotite + white mica-rich folia and polycrystalline quartz$_2$ ribbons. Menegon et al. (2006) estimated a minimum temperature of 450°–500 °C during shearing on the basis of: (i) the synkinematic metamorphic reactions, including the replacement of albite + epidote by oligoclase (Pryer, 1993); (ii) the extensive development of myrmekite (Vernon, 2004); and (iii) the strain-induced development of fine-grained aggregates of new K-feldspar (Fitz Gerald and Stünitz, 1993).

4. Analytical techniques

The microstructures of the Piantonetto protomylonites and mylonites were analysed by optical and scanning electron microscopy (backscattered electron, BSE, secondary electron, SE, and orientation contrast, OC). Image analysis was performed on BSE and OC images to calculate: (i) the average content of white mica in the protolith and in the mylonite; and (ii) the average orientation of the grain shape fabric of recrystallized K-feldspar within mylonite.

Crystallographic preferred orientation (CPO) of quartz and K-feldspar was measured by computer integrated polarization microscopy (CIP: Panozzo Heilbronner and Pauli, 1993; Heilbronner, 2000) and electron backscatter diffraction (EBSD: Prior et al., 1996), respectively. The input images for the CIP analysis were acquired by a Zeiss Axioplan microscope, equipped with a Zeiss AxioCam MRm digital camera. The EBSD patterns were acquired by a CamScan MX2500 SEM equipped with a tungsten filament and were indexed using Channel 5.0 software by HKL Technology. Indexing was accepted when at least six detected Kikuchi bands matched with those in the standard reflector file for orthoclase. Orientation contrast (OC) images were acquired using solid-state detectors in a forescatter position as described by Prior et al. (1996). A detailed description of the EBSD technique can be found in Prior et al. (1996).

5. Optical and SEM backscattered electron microstructures

Microstructures of the Piantonetto mylonites were investigated on thin sections cut orthogonal to the foliation and parallel to the stretching lineation. Further details on the microstructure of quartz, feldspars and, especially, myrmekites can be found in Menegon et al. (2006).

5.1. Quartz

Quartz within the mylonites consists of polycrystalline aggregates elongated in the foliation that were derived from the recrystallization of magmatic crystals. The recrystallized grains range in size from 100 to 400 μm and display sutured to serrated grain boundaries typical of grain boundary migration recrystallization (Fig. 2a). Local mica trails within the quartz bands cause frequent 'window'-microstructures by pinning migrating quartz grain boundaries (Jessel, 1987) (Fig. 2a).

5.2. Plagioclase

The magmatic plagioclase is replaced by a synkinematic fine-grained aggregate of plagioclase$_2$ + white mica + epidote ± garnet. The plagioclase within these aggregates has a composition ranging from albite to, more commonly, oligoclase. Oligoclase typically forms rims around albite grains and these rims grow preferentially in a direction parallel to the mylonitic foliation (Fig. 2b) (Menegon et al., 2006).

5.3. K-feldspar

K-feldspar porphyroclasts (Kfs_1) show pervasive cross-hatched twinning typical of microcline and, within the coarser porphyroclasts, exsolution lamellae of perthitic albite. Albite is present both as regularly spaced thin laths (a few microns to 200 μm in width) and as larger ribbons or patches, extending across the whole K-feldspar grain. Flame perthites are rare and they typically merge into albitic rims at microcline grain boundaries. Perthitic albite is mostly recrystallized to fine-grained (<10 μm–30 μm) polycrystalline bands, with individual albite grains rimmed by oligoclase. The oligoclase rims are thicker in the orientation parallel to the foliation, as also observed for plagioclase in the mylonitic matrix (Fig. 2b, see Section 5.2). Undulatory extinction of K-feldspar is particularly strong adjacent to both twinned domains and coarse patches of albite.

K-feldspar porphyroclasts are dissected by dilatant fractures oriented at a high angle to the mylonitic foliation and, less commonly, by conjugate shear fractures with an intersection angle of ~60° (Fig. 3a). Fractures are often developed along cleavage planes and twin boundaries and can either cut through the whole grain or terminate within the grain. During mylonitization the porphyroclast fragments are displaced along microfractures and fragments undergo subsequent cycles of fracturing until they reach a critical size of about 500 μm, after which further fracturing is uncommon (see Michibayashi,

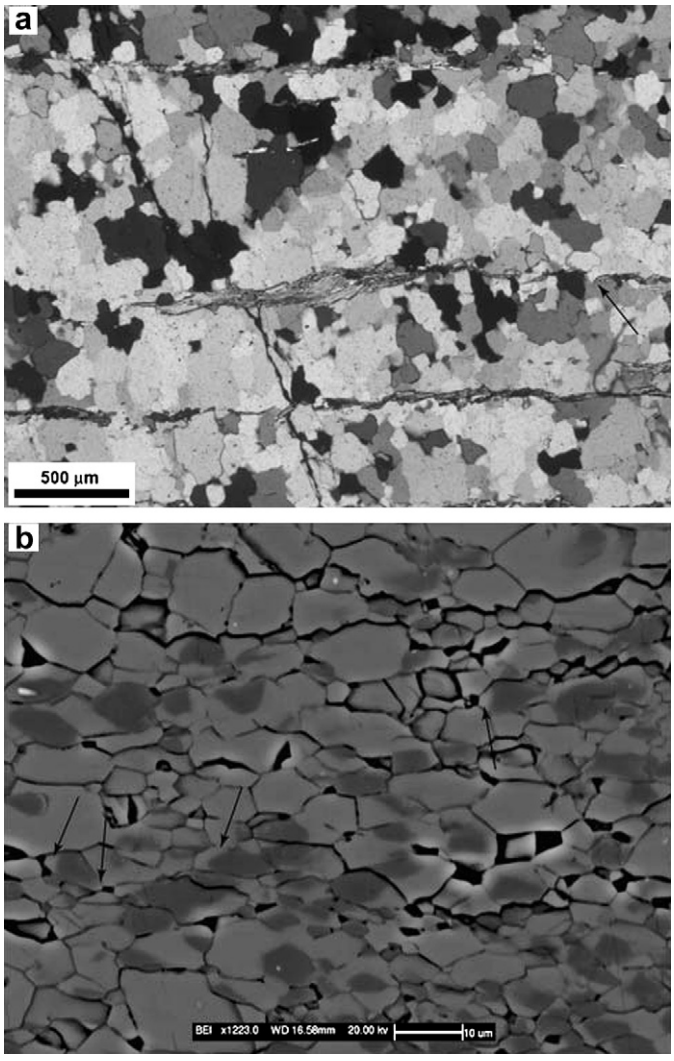

Fig. 2. (a) Optical microstructure of a polycrystalline aggregate of recrystallized quartz grains within the mylonitic sample P15Zc. Strongly irregular grain boundaries are evident. The black arrow indicates a typical ''window''-microstructure. Mylonitic foliation is oriented EW. Crossed polars. (b) SEM-BSE image of a fine-grained aggregate of recrystallized plagioclase along the mylonitic foliation, here oriented EW. Albite (dark grey) is progressively replaced by oligoclase (light grey) through the formation of rims preferentially elongated parallel to the foliation (see arrows).

1996). In the matrix surrounding the porphyroclasts, white mica-rich strain caps (Passchier and Trouw, 1996) are locally developed in the contractional quadrants of flow (Fig. 3b). Dilatant fractures within porphyroclasts, pull-aparts between displaced porphyroclasts (Fig. 3c) and pressure shadows around porphyroclasts are filled with elongated to, more rarely, fibrous K-feldspar$_2$ grains (Kfs$_{2\text{-EL}}$) and minor euhedral quartz$_2$ grains. The long axes of Kfs$_{2\text{-EL}}$ are preferentially aligned subparallel to the mylonitic foliation or to the local displacement direction joining pulled-apart K-feldspar fragments. The new grains are up to 300 µm long, are not perthitic, and mostly appear to be strain-free under the optical microscope (Fig. 3d). A few narrow (50–100 µm wide) bands of K-feldspar$_2$ within porphyroclasts consist of fine-grained aggregates of small (20 µm in diameter), equant K-feldspar$_2$ grains developed along incipient microcracks and twin boundaries (Fig. 4a). Similar to Kfs$_{2\text{-EL}}$, these bands display sharp boundaries to the host porphyroclasts, without transitional zones with optically visible subgrain structures. Microprobe analysis (on a Cameca Camebax of the C.N.R., at the Geosciences Department of Padova University) shows that these granoblastic K-feldspar$_2$ grains as well as Kfs$_{2\text{-EL}}$ are identical in composition to K-feldspar$_1$ (Or$_{95}$) (see Table 1 in Menegon et al., 2006).

The abundant precipitation of Kfs$_{2\text{-EL}}$ at all mylonitic stages is associated with extensive replacement of K-feldspar$_1$ by myrmekite (Menegon et al., 2006). Myrmekite nucleates along intragranular fractures and along the margins of albite lamellae or patches within large K-feldspar. It completely surrounds small porphyroclasts in the mylonitic matrix. Myrmekite grows in association with white mica, whose average content increases from 1.5 to 4% in volume in the metagranites to 2–9% in the mylonites, as estimated by image analysis on SEM photos. During the progressive deformation, myrmekite extensively recrystallizes to a granoblastic aggregate of oligoclase and quartz. Only very rarely does myrmekite replace non-perthitic Kfs$_{2\text{-EL}}$ grains.

During progressive mylonitization, different stages in the evolution of the K-feldspar domains can be recognized. At first, microcline porphyroclasts are dismembered along the network of through-going discrete micro-shear zones exploiting intragranular fractures, microveins and bands of recrystallized material (Fig. 4b). Then fractured Kfs$_1$ fragments are dispersed within millimetre-thick layers of fine-grained quartz-feldspar matrix representing the product of recrystallization and flow of myrmekites, of perthitic albite and of Kfs$_{2\text{-EL}}$ (Fig. 4c). Eventually, nearly monomineralic, 100–300 µm thick layers of granoblastic K-feldspar$_2$ develop, probably as a result of the ''recrystallization'' of the extensively precipitated Kfs$_{2\text{-EL}}$ grains (Figs. 4d,e). These layers contain a discontinuous foliation of white mica (Fig. 4d), a few small isolated porphyroclasts, and dispersed grains of quartz and/or plagioclase (Figs. 4d,f). The K-feldspar$_2$ grains are 20–50 µm in diameter and typically show a strong shape preferred orientation (SPO) inclined at about 25° with respect to the mylonitic foliation (Figs. 4d–f and 5). The average aspect ratio of the grains is 2.7, with values ranging from less than 2 to up to 7.

6. Grain boundary microstructure of K-feldspar: SEM-SE investigation

Secondary electron (SE) imaging of broken surfaces using a scanning electron microscope (SEM) is a simple but powerful technique for analyzing the grain boundary morphology of polycrystalline aggregates (Hippertt, 1994b; Mancktelow et al., 1998; Mancktelow and Pennacchioni, 2004). We used this method to investigate the grain boundary microstructure of recrystallized K-feldspar on differently oriented broken surfaces within K-feldspar$_2$ aggregates of the mylonite sample P15Z (Figs. 1b and 4e).

Slabs of a few millimetres thickness were cut parallel to the main sample reference axes (XY = mylonitic foliation, X = lineation) and were broken by hand approximately

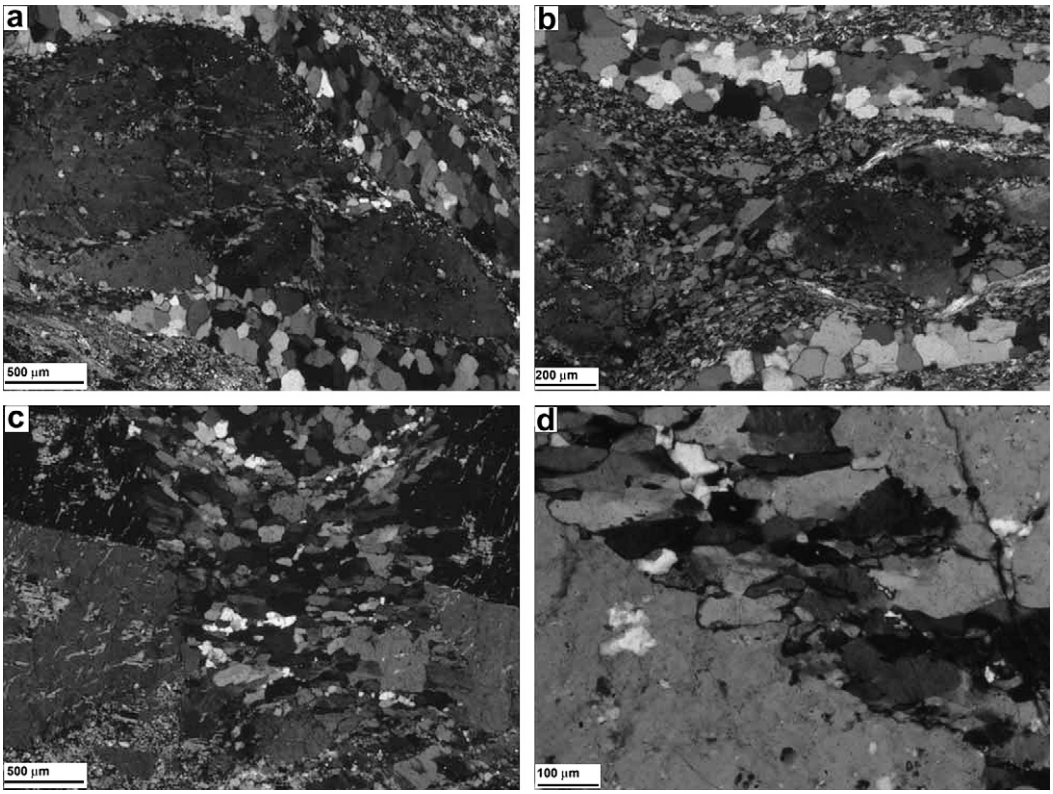

Fig. 3. Optical microstructures of dilatant sites within and around K-feldspar porphyroclasts. Bulk sense of shear is dextral in all examples. (a) Dilatant and conjugate fractures filled by elongated K-feldspar crystals. Bulk foliation oriented approximately NW-SE. Crossed polars. (b) Boudinaged K-feldspar porphyroclast. K-feldspar$_2$ and quartz are precipitated within the neck. On the opposite K-feldspar$_1$ surfaces, well-developed white mica-rich strain caps are evident. Bulk foliation oriented E-W. Crossed polars. (c) Micro pull-apart opening within a Carlsbad twinned K-feldspar porphyroclast elongated subparallel to the bulk foliation, oriented E-W. The filling consists of elongated K-feldspar$_2$ grains and quartz. The concavity of the internal foliation at the upper part of the neck is due to the tendency for the external polycrystalline matrix of recrystallized quartz to fill in the opening gap. Crossed polars. (d) Close-up of elongated K-feldspar$_2$ grains precipitated within a fracture. The grains are not perthitic and appear strain-free. Crossed polars.

parallel to XZ and YZ sections. The broken chips were coated with a 30 nm thick gold film and investigated under the SEM in SE mode using an acceleration voltage of 15–20 kV. Because the K-feldspar-rich ribbons also contain some quartz and plagioclase (Fig. 4f), energy dispersive spectroscopy (EDS) was used to identify mineral phases.

During breaking, the samples mostly parted along grain boundaries of recrystallized K-feldspar$_2$, and along intragranular fractures across K-feldspar$_1$ porphyroclasts (>50 μm in size). The broken surface is irregular at the grain scale and locally allows a 3D view of grain geometry. On ~XZ surfaces, K-feldspar$_2$ grains (~20–50 μm average grain size) are elongated at an angle of 10–40° to the mylonitic foliation, in a sense consistent with the bulk sense of shear. On ~XZ and XY surfaces, the grain boundaries are rarely smooth, well-developed crystal faces. Instead they are typically rough, due to the presence of pervasive bulges, ridges and depressions of submicron size (Figs. 6a–c). These topological features are irregular in size and distribution, but locally form orthogonal sets of structures that are most likely controlled by the orientation of cleavage planes (Fig. 6a). They are similar to the 'ridge and valley' grain boundary microstructure in quartz described by Hippertt (1994b) and Mancktelow and Pennacchioni (2004). In most cases, the grain boundary roughness matches the negative shape of the adjacent grain surface (Figs. 6b,d), indicating that these features represent irregular tight interfaces rather than open porosity.

On ~YZ surfaces, the grain boundary microstructure of K-feldspar is slightly different. The grain edges appear well-formed and most of them are perfectly straight. The two-grain interfaces are smoother than those observed on ~XZ planes, and the irregular 'ridge and valley' microstructure is less common (Figs. 6e,f). More typically, the ~YZ surfaces display two nearly orthogonal sets of second-order crystal facets (Figs. 6e,f) that closely resemble the {001} and {010} perfect cleavages of K-feldspar, in marked contrast to the corroded aspect observed on ~XZ and ~XY surfaces.

In addition to the topography described above, the grain boundaries in the different sections are characterized by the presence of sub-micron sized pores, often showing crystallographically-controlled, faceted shapes (e.g., triangular, arrowhead and lozenge shapes: Figs. 6c,d). These pores occur in regular geometric arrays and are similar to etch pits. This porosity decorates all the grain boundaries, independent on their orientation. Some isolated large pores (up to 4 μm, Fig. 6d) occur along intragranular fractures, as well as along grain edges and two-grain interfaces. Pores at triple junctions are also common (Fig. 6c).

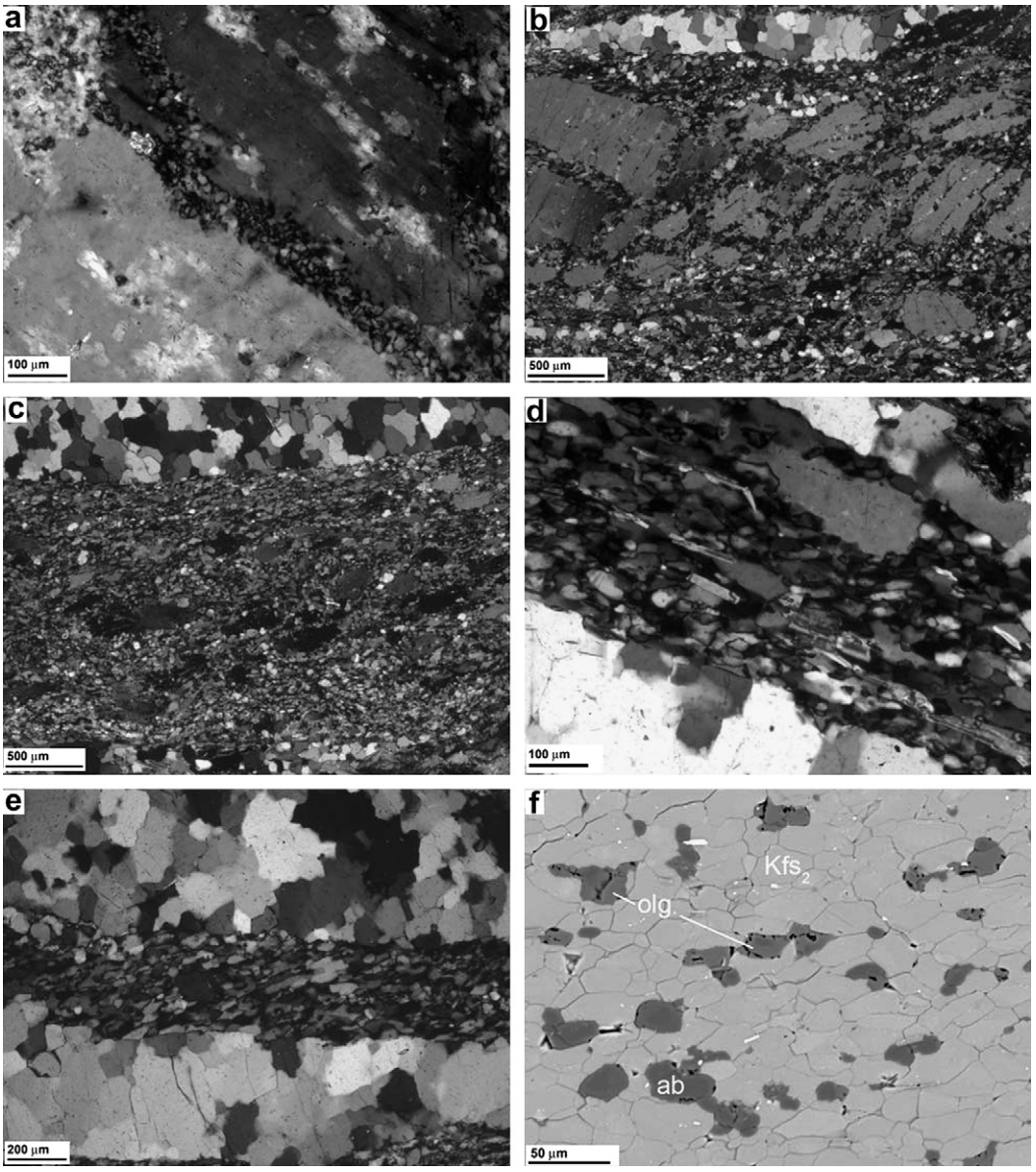

Fig. 4. Optical and backscatter electron (BSE) images of K-feldspar microstructure. Bulk sense of shear is dextral in all examples. (a) Fine-grained aggregate of new K-feldspar$_2$ localized on a Carlsbad twin boundary. Optical microscope, crossed polars. (b) Progressive grain size reduction of a K-feldspar porphyroclast occurring along a network of microveins and microshear zones. Optical microscope, crossed polars. (c) Advanced stage of K-feldspar grain size refinement. Single fragments ($\leq$500 μm in size) are incorporated within the mylonitic matrix without undergoing further fracturing. The matrix mostly consists of K-feldspar$_2$ grains, recrystallized myrmekite and recrystallized perthitic albite progressively re-equilibrating to oligoclase composition. The relative rotation of the individual porphyroclast fragments, originally belonging to a single grain, is reflected in their different interference colours. Optical microscope, crossed polars. (d) K-feldspar$_2$-rich layer along the mylonitic foliation, here running WNW-ESE. Small fragments of primary K-feldspar and a discontinuous foliation of white mica are evident. Note the shape preferred orientation of the K-feldspar recrystallized grains. Optical microscope, crossed polars. (e) Nearly monomineralic layer of K-feldspar$_2$ grains elongated parallel to the mylonitic foliation and confined between two polycrystalline ribbons of recrystallized quartz. Within the foliation-parallel layer, the K-feldspar$_2$ grains display a clear shape preferred orientation inclined at $\sim 10^\circ$–40° to the shear plane. (f) SEM backscattered electron image of a nearly monomineralic layer of K-feldspar$_2$ along the mylonitic foliation. Kfs$_2$ = K-feldspar$_2$, ab = albite, olg = oligoclase. K-feldspar$_2$ grains show abundant triple junctions at $\sim 120^\circ$ and a shape preferred orientation synthetically inclined at $\sim 10^\circ$–40° to the mylonitic foliation.

7. CPO analysis

7.1. Quartz

The CIP analysis of quartz c-axis CPO has been performed on a millimetre-thick completely recrystallized aggregate within sample P15Zc (Fig. 2a). The c-axis pole figure is shown in Fig. 7. The CPO pattern can be roughly classified as a type-II crossed girdle (Lister, 1977; Passchier and Trouw, 1996), with sharper maxima at the periphery of the pole figure and at a high angle to the foliation. The quartz c-axis CPO of sample P15Z is consistent with the dominant activity of basal ⟨a⟩ slip, with minor activity of rhomb ⟨a⟩ and prism ⟨a⟩ slip during recrystallization-accommodated dislocation creep.

Table 1
Active slip systems in K-feldspar, as compiled from the literature

Reference	Conditions	Slip plane	Slip direction	Method of observation
Experimental deformation:				
Tullis and Yund (1977)	900–1000 °C, 10–15 kb, 10^{-6}/s	(010)	Not determined	TEM
Willaime et al. (1979) and Scandale et al. (1983)	700 °C, 15 kb, 10^{-6}/s.	(010)	[101]	TEM
		(001)	½[110]	
		(1-2-1)	[101]	
		(010)	[001]	
		(110)	½[1-12]	
		(1-11)	½[110]	
	900 °C, 15 kb, 10^{-6}/s	(010)	[101]	
		(001)	½[110]	
		(1-2-1)	[101]	
		(010)	[100]	
Natural deformation:				
Debat et al. (1978)	550 °C, 2 kb	(010)	Not determined	OM
		(110)	Not determined	
Sacerdoti et al. (1980)	500 °C, 2 kb	(12-1)	[101]	TEM
		(010)	[101]	
		(010)	[100]	
		(010)	[001]	
		(010)	½[1-12]	
Schulmann et al. (1996)	550–600 °C, 4–8 kb	(010)	[001]	U-stage
		(010)	[100]	
Martelat et al. (1999)	700–800 °C, 4–10 kb	(010)	[100]	U-stage
		(001)	[100]	
Franek et al. (2006)	700–800 °C, 5–8 kb	(010)	[001]	EBSD
Ishii et al. (2007)	Upper greenschist facies	(100)	[010]	EBSD
		(101)	[010]	

The experiments of Tullis and Yund (1977) were conducted on dry Westerly granite (containing microcline); the experiments of Willaime et al. (1979) and Scandale et al. (1983) were conducted on single crystals of sanidine (Or_{80}). Slip systems inferred from U-stage and EBSD measurements are deduced from the CPO patterns. Slip planes inferred from optical microscope observations (OM in the table) are deduced from the occurrence of kink bands and albite gashes parallel to the specific crystallographic planes.

7.2. K-feldspar

EBSD analysis has been performed on the protomylonitic sample P3G and on the mylonitic sample P15Zc. Crystallographic orientations were collected from three distinct microstructural domains: (1) K-feldspar porphyroclasts within the protomylonite; (2) K-feldspar elongated grains within a dilatant site in the protomylonite; and (3) layers of recrystallized K-feldspar grains along the mylonitic foliation. For reference, the most common slip systems reported in the literature for potassic feldspars are listed in Table 1.

In some cases, e.g. for the two parts of Carlsbad twins, the Channel 5.0 program proposes two indexing solutions that are rotated about the [001] axis by 180° and differ only slightly in the mean angular deviation (MAD). In these cases we always chose the first solution, unless there was a clear reason for choosing another solution with a higher MAD-value (e.g. a better fit to the Kikuchi bands). Mis-indexing in such situations does not influence the orientation of the poles to the (100) and the (010) planes or the [010] and [001] directions, but does influence the position of the [100] and the [101] directions, as well as the position of the poles to the (001) planes. In fact, they will be rotated away from their true position by about 50° (Fig. 8). We cannot exclude the possibility that some of the data dispersion is an artefact resulting from mis-indexing.

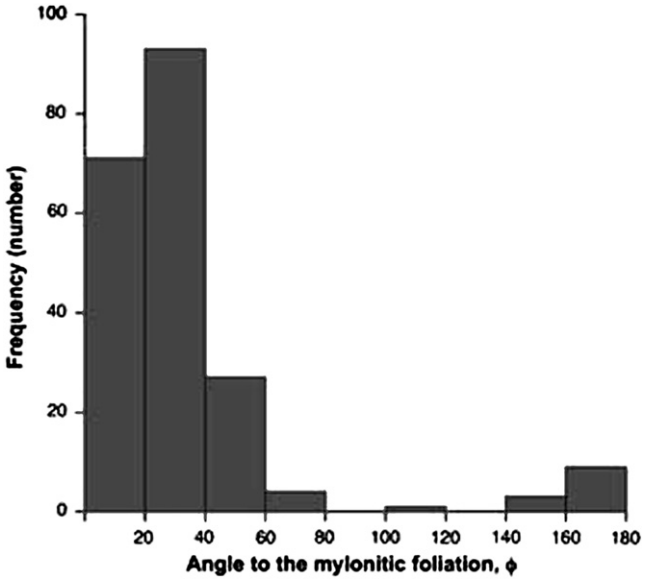

Fig. 5. Frequency distribution of the inclination of the long axis of single K-feldspar$_2$ grains within the layer of Fig. 4e, with respect to the shear plane ($n = 208$). The single grains were manually outlined on SEM BSE and OC images of different portions of the same layer. The aspect ratio of single grains and the inclination of the long axis have been measured by image analysis and approximated as those of the best-fit ellipses (software Image SXM: http://www.liv.ac.uk/~sdb/ImageSXM/). The angle is measured in an anticlockwise sense from the trace of the mylonitic foliation.

7.2.1. K-feldspar porphyroclasts

The crystallographic orientation of 44 K-feldspar porphyroclasts has been measured in sample P3G (protomylonite), which has a solid-state foliation defined by: (i) the alignment of biotite grains; (ii) the elongation of aggregates replacing plagioclase; and (iii) by recrystallized quartz domains. In this sample, the K-feldspar porphyroclasts are up to 0.5 cm in size and show micro-veins and micro-pull-apart openings. The crystallographic orientation of the porphyroclasts scatters across the entire pole figure (Fig. 9), without any clear CPO, which suggests the lack of any significant intragranular crystal plasticity in the K-feldspar.

7.2.2. K-feldspar elongated grains within a dilatant site

The orientation contrast images and EBSD data for new K-feldspar grains crystallized inside the neck of the fractured, boudinaged K-feldspar porphyroclast in sample P3G (protomylonite, Fig. 3c) are shown in Fig. 10. The $Kfs_{2\text{-}EL}$ aggregate within the neck has a double concave shape due to embayment of the mylonitic matrix during boudinage and separation of the porphyroclast fragments. The elongate grains define a straight foliation in the central part of the neck, directly connecting points of the porphyroclast walls that were originally in

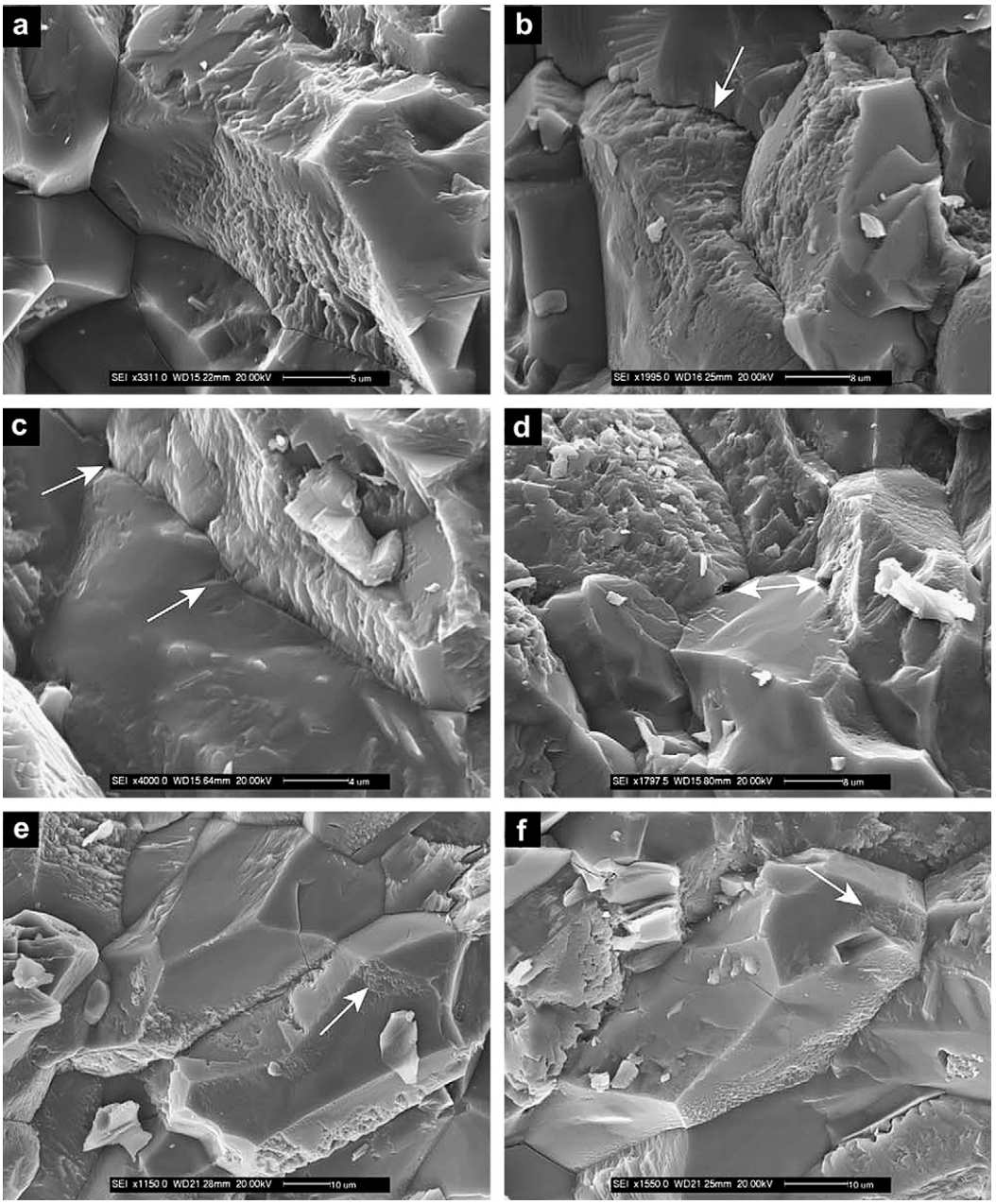

Fig. 6. SEM secondary electron (SE) images of broken surfaces for the mylonitic sample P15Z. (a–d) K-feldspar grain boundary microstructure on ~XZ surfaces. The bulk foliation runs N-S. (a) Network of ridges, bulges and depressions (i.e., 'ridge and valley' microstructure) on a K-feldspar grain boundary. These features are likely to be crystallographically-controlled, with the development of second order crystal facets. (b) Details of the rough and corroded grain boundary topography. Note the good match between the topographical irregularities on opposing grain surfaces (see white arrow). (c) Arrowhead-shaped pores (lower arrow), possibly along an intergranular fracture, and pore at triple junction (upper arrow). (d) Large (up to 3–4 μm) faceted cavities along two-grain interfaces (arrow). Note the pervasive occurrence of the corroded topography on differently oriented grain boundaries. (e, f) K-feldspar grain boundary microstructure on ~YZ surfaces. The bulk foliation runs E-W. (e) and (f) Relatively smooth grain boundary morphology, with the tendency to form two nearly orthogonal sets of steps (arrow), which possibly represent incipient growth by crystallographically controlled accretion. On these surfaces, well-developed 'ridge and valley' microstructures are rare.

contact (e.g. the point of intersections of Carlsbad twinning with the porphyroclast walls). They define a curved foliation toward the outer part of the neck due to distortion during embayment. The crystallographic orientation of 107 new grains within the neck and of flanking K-feldspar porphyroclast fragments (6 indexed points) is reported in Figs. 10c,d. These data clearly indicate a control of the crystallographic orientation of the host porphyroclasts on the CPO of $Kfs_{2\text{-EL}}$. The distortion of the K-feldspar aggregate toward the outer parts of the neck may in part account for the mismatching of $Kfs_{2\text{-EL}}$ orientations with respect to those of the host porphyroclast. The preferred epitaxial growth of $Kfs_{2\text{-EL}}$ is evident in the OC images in Figs. 10a,b. These images also show that there is no clear substructure or evidence for progressive misorientation of

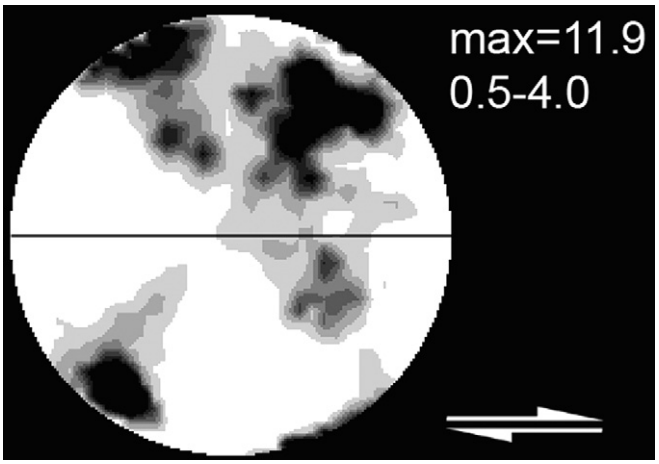

Fig. 7. CIP derived c-axis pole figure of recrystallized quartz grains in the mylonitic sample P15Zc. Equal area projection, upper hemisphere. The horizontal axis represents the trace of the mylonitic foliation and is parallel to the stretching lineation. Shear sense, maximum of the pole figure and shading intervals are indicated on the right.

the crystal lattice within the host porphyroclast toward the wall of the micro pull-apart.

7.2.3. Layers of recrystallized K-feldspar

We measured the crystallographic orientation of recrystallized K-feldspar$_2$ grains within nearly monomineralic layers of the mylonitic foliation (Fig. 4e). The K-feldspar$_2$ grains have a preferential shape orientation inclined at an average angle of about 25° to the mylonitic foliation (see Fig. 5 and orientation contrast images in Figs. 11a,b), with a monoclinic symmetry consistent with the dextral shear sense of the mylonite.

The crystallographic orientation of K-feldspar was measured in two distinct microstructural sites within the same thin section (Figs. 11a,b) for a total of 635 grains (290 from the site of Fig. 11a and 345 grains for the site of Fig. 11b). The K-feldspar shows the same CPO in both sites and the cumulative pole figure is shown in Fig. 11c. The CPO is weak, but with a preferred orientation especially evident for the poles to the (001) planes and the [100] and [001] crystallographic axes. The (001) poles and [001] axes are concentrated about the centre of the pole figure, whereas the [100] crystallographic axes concentrate near the primitive great circle, have a small maximum at 260°/20°, and a low density between 330° and 360°.

The arrangement of (100) poles can be interpreted as a combination between: (i) a preferred distribution in the NE and SW sector along the primitive circle; and (ii) a distribution along a SE dipping great circle. The poles to the (010) planes are instead distributed along a NW dipping great circle that has a marked maximum in the NW sector. Overall, this suggests that a significant proportion of (010) and (001) planes – and a significantly smaller proportion of (100) planes – form traces that are sub-parallel to the shape preferred orientation of the recrystallized K-feldspar grains imaged in Figs. 11a,b, whereas many (100) planes are preferentially oriented orthogonal to this shape preferred orientation.

8. Discussion

8.1. Intragranular crystal plasticity vs. dissolution-precipitation creep in K-feldspar

Under geological conditions, the crystal plastic deformation of K-feldspar becomes effective at ≥400–450 °C (Fitz Gerald and Stünitz, 1993 and references therein). In the Piantonetto granite mylonites, the synkinematic metamorphic temperatures have been estimated at ≥450–500 °C (Menegon et al., 2006), so that dislocation creep of K-feldspar might potentially be active. Indeed, Ishii et al. (2007) have demonstrated that dislocation creep can produce a CPO in K-feldspar

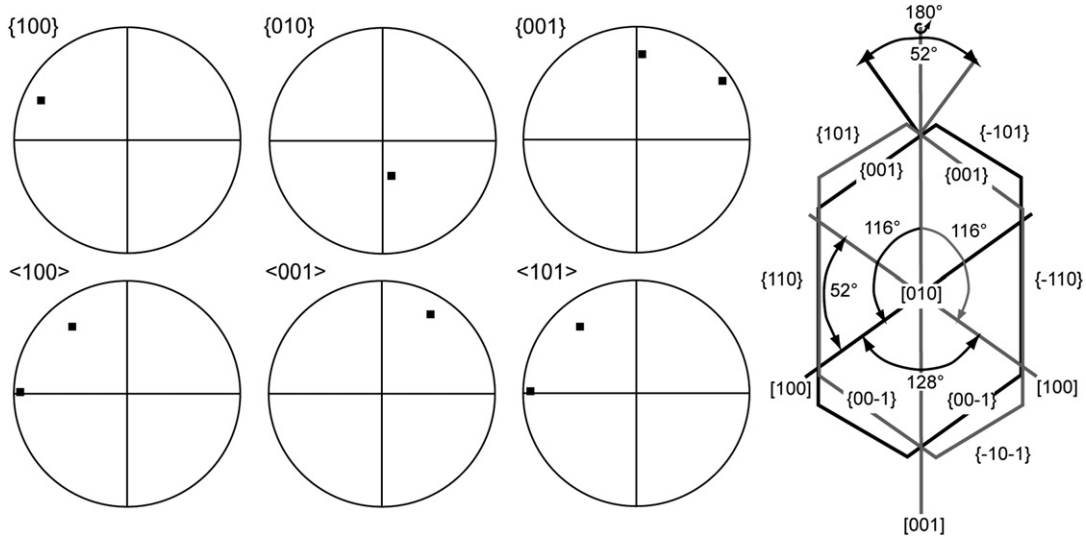

Fig. 8. Lower hemisphere, equal area projection of two possible solutions of the same analytical point, the second rotated by 180° about the [001] axis, as shown in the sketch on the right.

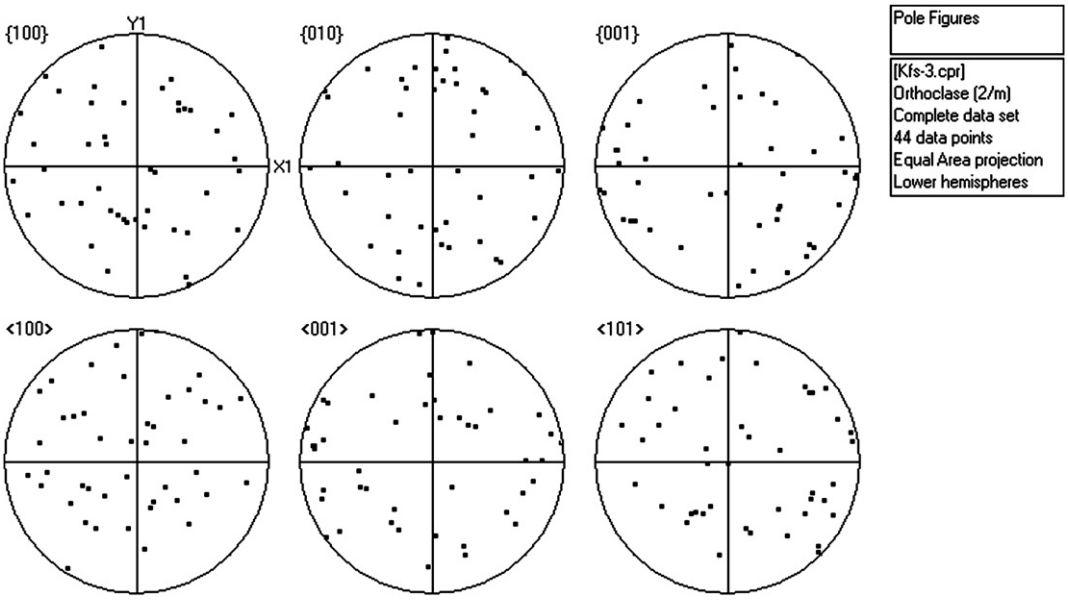

Fig. 9. Pole figures showing the crystallographic orientation of 44 K-feldspar porphyroclasts in the protomylonite P3G, derived from EBSD measurements.

aggregates in granitoids deformed under similar temperature conditions to those in the Piantonetto mylonites.

However, crystal plasticity and recovery processes in K-feldspar from the Piantonetto mylonites were probably negligible, as suggested by the absence of: (i) a CPO of K-feldspar porphyroclasts in the protomylonite (Fig. 9); (ii) a CPO in recrystallized aggregates consistent with known active slip systems in K-feldspar (see below); and (iii) subgrain microstructures in OC images of porphyroclasts (Figs. 10a,b). In contrast, fluid-present conditions and significant dissolution/precipitation during deformation are suggested by several observations: (i) the extensive development of myrmekite; (ii) the extensive precipitation of K-feldspar $\pm$ quartz within dilatant domains; (iii) the grain boundary microstructure of K-feldspar$_2$ grains; and (iv) the local formation of white mica-rich strain caps at high normal stress sites around porphyroclasts, suggestive of the removal of more soluble material (e.g., Blenkinsop, 2000). The strong SPO of Kfs$_2$ aggregates within the mylonites is possibly further evidence for the activity of stress-induced solution transfer. Grain shape fabrics might form by dissolution-precipitation creep during simple shear deformation even at low shear strain values (Blenkinsop, 2000; Bons and den Brok, 2000). This can result from a balance between the precipitation of new material (which reflects only the last increment of strain) and the progressive rotation of the newly formed grains towards the shear plane. Dissolution-precipitation was also active during plagioclase deformation, as indicated by the asymmetry of oligoclase overgrowths on albite grains in the recrystallized aggregates (Fig. 2b; Menegon et al., 2006). The irregular lobate optical grain boundary microstructure of recrystallized quartz is also consistent with fluid-assisted high grain boundary mobility (e.g., Urai et al., 1986; Mancktelow and Pennacchioni, 2004). Mancktelow et al. (1998) showed that this optical microstructure consists, under the SEM, of a series of straight crystal faces that most likely developed by growth in a fluid-rich environment.

The stored strain energy within K-feldspar porphyroclasts derives both from stress concentration due to matrix flow around the porphyroclasts and from the extensive microcline twinning and microperthitic texture (Fitz Gerald and McLaren, 1982; Pryer and Robin, 1996; Menegon et al., 2006). The lattice distortion mainly drives the replacement of K-feldspar by myrmekite, which occurs pervasively at all stages of deformation. Myrmekite formation is consistent with the widespread deposition of K-feldspar new grains from the grain boundary fluid phase, which represents a major sink for the K ions removed from the reaction site. In addition, it may partially account for the slight increase in the content of white mica from the weakly deformed protolith to the granite mylonite. Myrmekite replacement was estimated to occur in the presence of $\sim$1 wt% of fluid (Menegon et al., 2006).

The pervasive preferential occurrence of corroded grain boundaries on $\sim$XY and $\sim$XZ surfaces (Figs. 6b,c) within recrystallized K-feldspar$_2$ aggregates, and the perfect matching between adjacent corroded surfaces (Figs. 6b,d), might be taken as indicative of dissolution processes along grain boundaries oriented at a high angle to the shortening direction (Hippertt, 1994b; Mancktelow et al., 1998; Mancktelow and Pennacchioni, 2004). The smoother surface of grain boundaries (Figs. 6e,f) and the presence of new crystal facets on $\sim$YZ surfaces suggests both the absence of important dissolution and crystallographically-controlled growth in a direction subparallel to the extensional direction (Blenkinsop, 2000; Mancktelow and Pennacchioni, 2004), as expected for stress-induced solution transfer. In the Piantonetto mylonites, we therefore conclude that dissolution, replacement and precipitation processes were dominant during deformation of K-feldspar under temperature conditions where dislocation creep could be expected.

The presence of about 1 wt% of aqueous fluid during mylonitization of the Piantonetto metagranite (Menegon et al., 2006) might account for the dominance of dissolution-precipitation

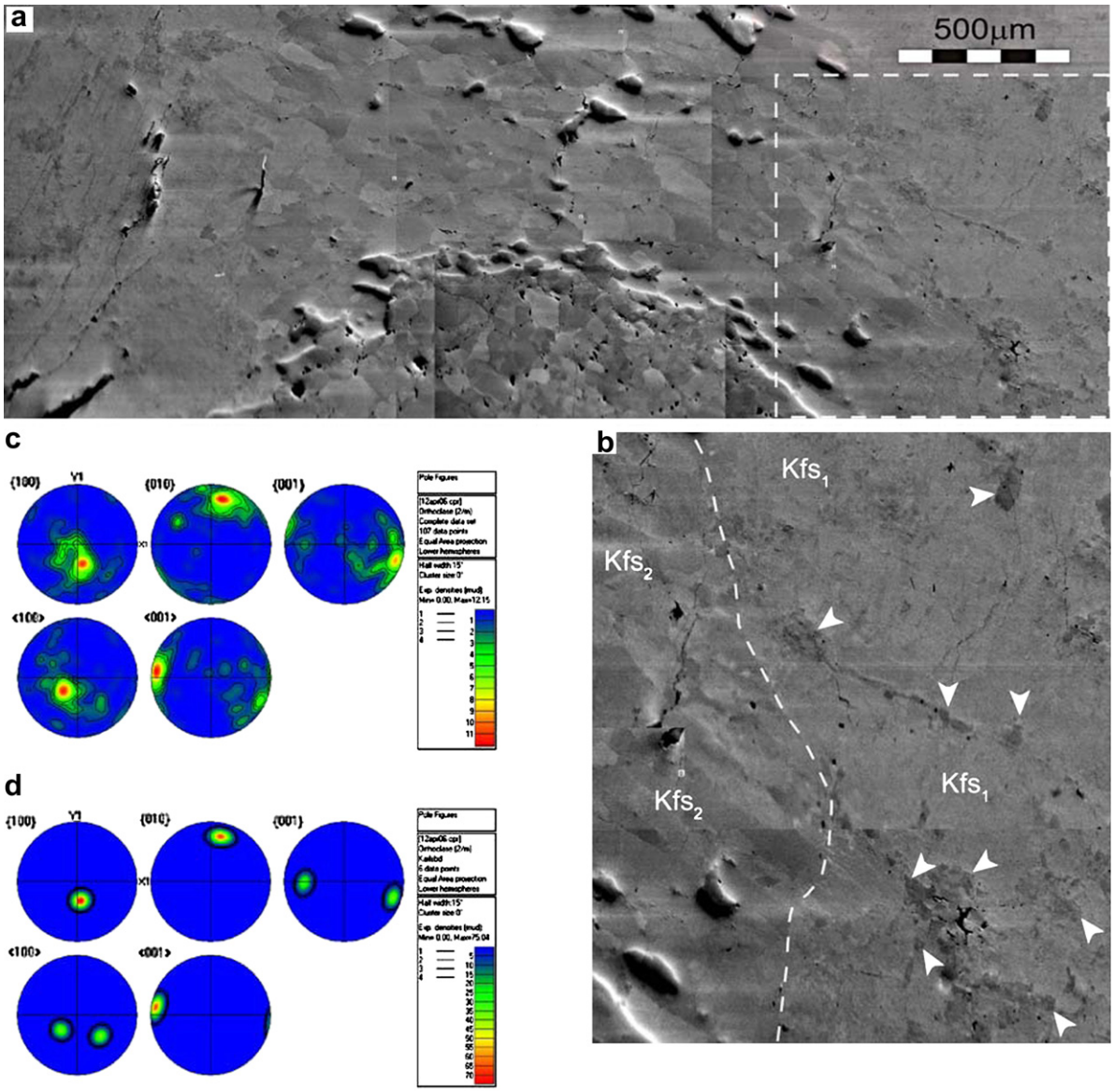

Fig. 10. (a) Orientation contrast image of a portion of the micro pull-apart opening shown in Fig. 3c. With respect to Fig. 3c, the image is rotated through 180°. The white dashed rectangle is the area shown in detail in b. (b) Detail of the lower-right portion of a. The image shows the lack of subgrain microstructures within the K-feldspar$_1$ porphyroclast. The white dashed line outlines the pull-apart wall. White arrows indicate lamellae and patches of albite. (c) Pole figures showing the orientation of new K-feldspar grains precipitated within the neck, relative to the orientation of the two parts of the Carlsbad twin (d), derived from EBSD measurements. Sense of shear is dextral.

creep over dislocation creep. This is in agreement with the experimental work of Tullis et al. (1996), who observed that the deformation of orthoclase aggregates was accompanied by an enhanced fluid distribution throughout the whole sample, promoting a switch from dislocation creep to pressure solution. Given the small amounts of intergranular fluid (<1 wt%) needed to induce this change in the dominant deformation mechanism, Tullis et al. (1996) concluded that the same change is very likely to occur also under mid-crustal conditions. Deformation by dominant dissolution-precipitation of orthoclase, as well as of other rock forming minerals, is well established for granitoids under water-present mid-crustal conditions (e.g., Wintsch and Yi, 2002).

During plastic deformation of minerals, stress-induced solution transfer is known to occur at lower differential stress/strain rates than dislocation creep (e.g., Rutter, 1976; Passchier and Trouw, 1996). The prominent role of dissolution-precipitation during deformation of K-feldspar in the Piantonetto mylonites might therefore reflect lower differential stress/strain rates compared to the Ryoke mylonites, Japan, described by Ishii et al. (2007) where, under metamorphic conditions similar to Piantonetto, dislocation creep is the dominant deformation mechanism.

8.2. Development of a CPO in K-feldspar by dissolution-precipitation creep

The presence of a CPO within a recrystallized aggregate and the alignment of crystallographic planes and axes with the shear plane and direction are commonly interpreted as evidence for crystal plastic behaviour due to dislocation creep (Schmid

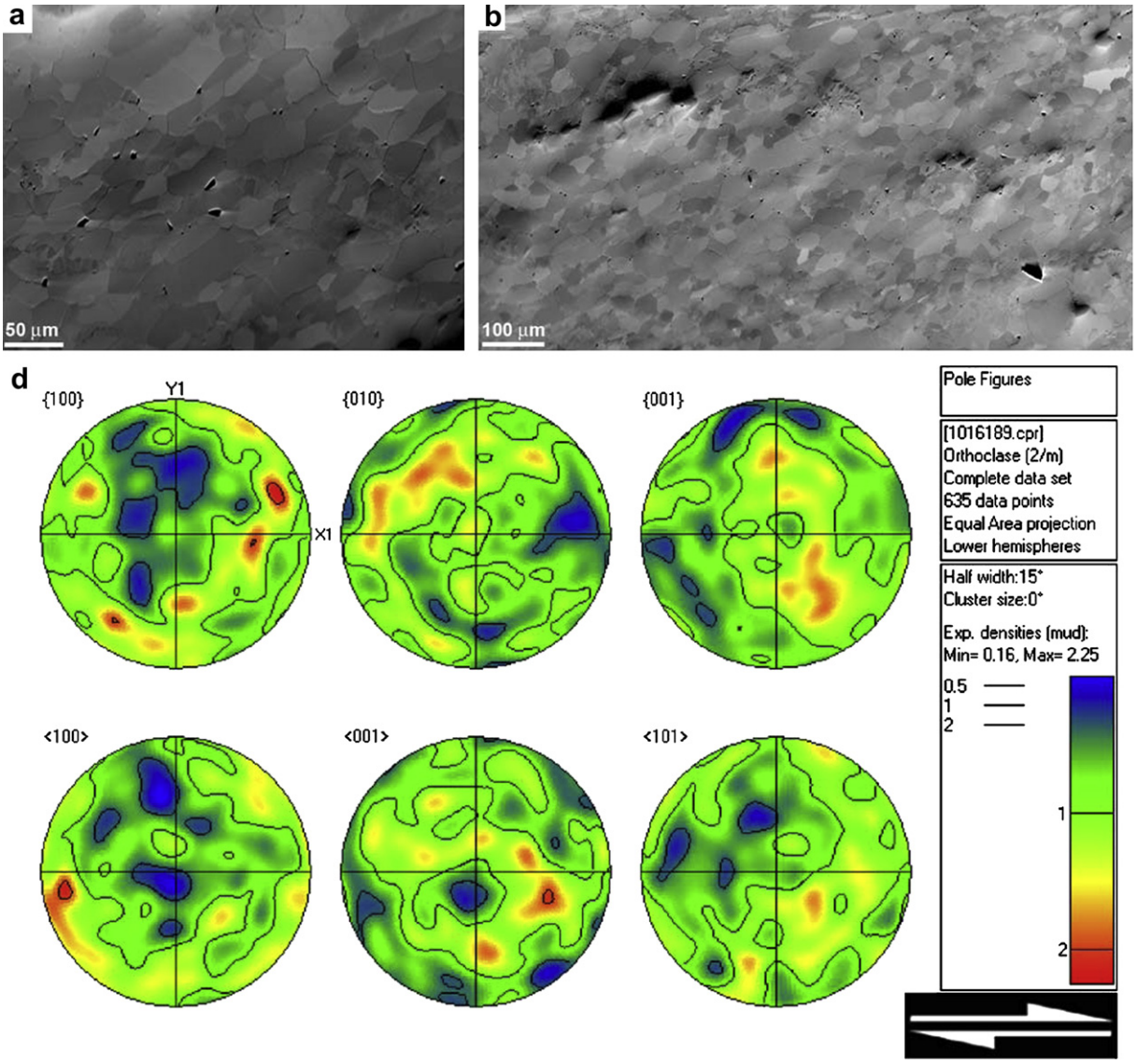

Fig. 11. (a, b) Orientation contrast images of recrystallized K-feldspar bands in the two analyzed microstructural sites. Mylonitic foliation in thin section is oriented E-W. In both sites, K-feldspar grains show a preferred shape orientation oblique to the mylonitic foliation and running NE-SW to ENE-WSW. (c) Pole figures showing the crystallographic orientation of recrystallized K-feldspar grains derived from EBSD measurements. Dextral sense of shear. One point per grain was analyzed.

and Casey, 1986; Passchier and Trouw, 1996). In the case of K-feldspar, experimental studies (Tullis, 1983 and references therein) and the analysis of recrystallized natural aggregates (Debat et al., 1978; Sacerdoti et al., 1980; Schulmann et al., 1996; Martelat et al., 1999; Franek et al., 2006; Ishii et al., 2007) have shown that the most common active slip plane over a wide range of conditions is (010) and that slip directions are [101], [100], [001] and [010] (Table 1). Therefore, if dislocation creep was the dominant deformation mechanism in K-feldspar$_2$ aggregates of Piantonetto mylonites, (010) planes should be preferentially aligned parallel to the foliation. This is not the case and indeed no other crystallographic plane appears to be well oriented for slip along the foliation. The pole figures instead show a weak preferred orientation of [100] axes rotated anticlockwise relative to the foliation in the XZ plane (Fig. 11c) and do not appear to be consistent with any known slip system (Table 1). We interpret this CPO as the result of dominant dissolution-precipitation creep.

Anisotropic growth is common in minerals and can produce an SPO and a CPO during deformation simply by rigid body rotation (e.g., Berger and Stünitz, 1996), which tends to align the long axis of crystals with the extensional instantaneous stretching axis or ISA (Passchier and Trouw, 1996). During pressure solution, minerals can display different rates of surface reactivity (or dissolution/growth rate) along different crystallographic directions (e.g., quartz: Becker, 1995; Den Brok, 1996; mica: Etheridge et al., 1974; Mancktelow, 1979). Irrespective of the presence of a strong shape anisotropy, the crystallographically-controlled anisotropy in reaction rate may also play a role, producing a CPO with the faster

growth direction aligned with the extensional ISA (e.g., Hippertt, 1994a; Godard and van Roermund, 1995; Takeshita and Hara, 1998; Bons and den Brok, 2000). The numerical modelling of Bons and den Brok (2000) demonstrated that a combination of dissolution-precipitation creep with rigid body rotation of mineral grains can produce a CPO in a deforming aggregate at low shear strain values ($\gamma \leq 3$) and for a range of different deformation geometries (simple shear, uniaxial shortening, plane strain pure shear). In these numerical models, grains preferentially ended up with the crystallographic axis with the slowest and highest reaction rate oriented parallel to the maximum shortening and extension direction, respectively. The CPO patterns obtained in these models are similar to those observed in natural and experimental deformation in which dissolution-precipitation creep was operative (e.g., Hippertt, 1994a; Takeshita and Hara, 1998; Heidelbach et al., 2000).

If dissolution-precipitation creep is mainly responsible for the development of the CPO in the K-feldspar$_2$ aggregates in the Piantonetto mylonites, then: (i) the fast reaction rate should be parallel to [100]; and (ii) the slow reaction rate should be parallel to [010] and [001]. Grains with (100) planes orthogonal to the instantaneous shortening axis should be preferentially dissolved, and grains with (100) planes in a direction perpendicular to the extensional ISA should grow faster. The grain boundary microstructure of K-feldspar as seen on ~YZ surfaces lends support to this interpretation. The common occurrence of two nearly orthogonal sets of steps on grain boundaries facing the extension direction (Figs. 6e,f) could be related to the preferred growth of (010) and (001) planes (i.e., planes parallel to the [100] axis), corresponding to the perfect cleavages in K-feldspar.

In early stages of deformation, the development of a bulk CPO in the Kfs$_2$ aggregates is inhibited by the strong epitaxial control on the crystallographic orientation of new grains exerted by parent porphyroclasts. The initial random orientation of K-feldspar$_1$ crystals (Fig. 9), the absence of significant crystal plasticity within porphyroclasts, and the continuous fragmentation and rotation of K-feldspar clasts during flow tend to randomize the bulk crystallographic orientation of the new grains. This effect is also promoted by the strong perturbation in flow streamlines induced by the presence of porphyroclasts. The process of randomization eventually becomes subordinate at very high strain after dismembering and consumption of most porphyroclasts, essentially through the process of myrmekite formation and associated K-feldspar precipitation. It is however worth noting that K-feldspar is the most abundant mineral in the granite (37% volume) and porphyroclasts persist to high strain.

The weak CPO measured in the Kfs$_2$ from the mylonites cannot be simply explained by continuous randomization as discussed above. The investigated aggregates of sample P15Z (Figs. 4e and 11a,b) are virtually free of relict porphyroclasts. The weakness of the CPO developed by dissolution-precipitation creep is probably related to a low anisotropy in the crystallographically-controlled reaction rate (or dissolution/growth rate) of K-feldspar.

9. Conclusions

Within the lower amphibolite facies granite mylonites of the Piantonetto Valley (Gran Paradiso nappe of the North-Western Alps), K-feldspar occurs in fine-grained polygonal aggregates forming nearly monomineralic layers elongated along the foliation. Within these layers, K-feldspar has a weak CPO that is not consistent with the activity of known slip systems in K-feldspar. This suggests that dislocation creep was not the dominant deformation mechanism. The observed CPO can best be explained by dissolution-precipitation creep characterized by a fast reaction rate parallel to [100] and a slow reaction rate parallel to [010] and [001]. The weakness of the CPO indicates a low crystallographically-controlled anisotropy in reaction rate of K-feldspar.

In the studied rocks, dissolution-precipitation processes and grain-scale fluid-assisted mass transfer are well documented by the development of myrmekite and by the extensive epitaxial growth of K-feldspar grains within dilatant domains associated with K-feldspar porphyroclasts from the earliest stages of progressive mylonitization. For a relatively high porphyroclast/precipitated grains ratio, epitaxial growth of new K-feldspar grains hinders the achievement of a CPO and tends to randomize the orientation of new grains. At a low porphyroclast/precipitated grains ratio, dissolution-precipitation creep prevails and produces a weak CPO, with selective growth and dissolution of grains within the nearly monomineralic mylonitic layers. Under mid-crustal conditions and at temperatures consistent with the activation of dislocation creep in feldspars, dissolution-precipitation creep can play a primary role both in the accommodation of deformation and in the development of a CPO in K-feldspar aggregates.

Acknowledgements

This study has been funded by the University of Padova (i) Progetto di Ateneo 2003; and (ii) Ricerca Scientifica fondi quota ex 60% (60A05-3129/05 and 60A05-3770/06). The paper was substantially improved thanks to the constructive review of T. Takeshita and to additional comments by R. Wintsch. J. Hippertt is acknowledged for editorial handling. We thank Holger Stünitz for his critical pre-reading, Neil Mancktelow for further remarks and improvement of the English, and Renee Heilbronner for making available the CIP facilities at the University of Basel. The Parco Nazionale del Gran Paradiso is kindly acknowledged for providing logistical support during field work and for allowing rock sampling.

References

Altenberger, U., Wilhelm, S., 2000. Ductile deformation of K-feldspar in dry eclogite facies shear zones in the Berge Arcs, Norway. Tectonophysics 320, 107–121.

Álvarez-Valero, A.M., Cesare, B., Kriegsman, L.M., 2005. Formation of elliptical garnet in a metapelitic enclave by melt-assisted dissolution and reprecipitation. Journal of Metamorphic Geology 23, 65–74.

Ballèvre, M., 1988. Collision continentale et chemins P-T. L'unité Pennique du Grand Paradis (Alpes Occidentales). Mémoires et Documents du Centre Armoricain d'Etude Structurale des Socles 19. Rennes, France.

Becker, A., 1995. Quartz pressure solution: influence of crystallographic orientation. Journal of Structural Geology 17, 1395–1405.

Berger, A., Stünitz, H., 1996. Deformation mechanisms and reaction of hornblende: examples from the Bergell tonalite (Central Alps). Tectonophysics 257, 149–174.

Blenkinsop, T., 2000. Deformation Microstructures and Mechanisms in Minerals and Rocks. Kluwer Academic Publishers.

Bons, P., den Brok, B., 2000. Crystallographic preferred orientation development by dissolution-precipitation creep. Journal of Structural Geology 22, 1713–1722.

Borghi, A., Compagnoni, R., Sandrone, R., 1996. Composite P-T paths in the Internal Penninic Massifs of the Western Alps: petrological constrains to their thermo-mechanical evolution. Eclogae Geologicae Helvetiae 89/1, 345–367.

Callegari, E., Compagnoni, R., Dal Piaz, G.V., 1969. Relitti di strutture intrusive e scisti a sillimanite nel Massiccio del Gran Paradiso. Bollettino della Società Geologica Italiana 88, 59–69.

Dal Piaz, G.V., Lombardo, B., 1986. Early Alpine eclogite metamorphism in the Penninic Monte Rosa-Gran Paradiso basement nappes of the northwestern Alps. In: Evans, B.W., Brown, E.H. (Eds.), Blueschists and Eclogites. Geological Society of America Memoires 164, 249–265.

Dal Piaz, G.V., Hunziker, J.C., Martinotti, G., 1972. La zona Sesia-Lanzo e l'evoluzione tettonico-metamorfica delle Alpi nordoccidentali interne. Memorie della Società Geologica Italiana 11, 433–462.

Debat, P., Soula, J.-C., Kubin, L., Vidal, J.-L., 1978. Optical studies of natural deformation microstructures in feldspars (gneiss and pegmatites from Occitania, southern France). Lithos 11, 133–145.

Den Brok, B., 1996. The effect of crystallographic orientation on pressure solution in quartzite. Journal of Structural Geology 18, 859–860.

Etheridge, M.A., Paterson, M.S., Hobbs, B.E., 1974. Experimentally produced preferred orientation in synthetic mica aggregates. Contributions to Mineralogy and Petrology 44, 275–294.

Fitz Gerald, J.D., McLaren, A.C., 1982. The microstructure of microcline from some granitic rocks and pegmatites. Contributions to Mineralogy and Petrology 80, 219–229.

Fitz Gerald, J.D., Stünitz, H., 1993. Deformation of granitoids at low metamorphic grade. I: Reactions and grain size reduction. Tectonophysics 221, 269–297.

Franek, J., Schulmann, K., Lexa, O., 2006. Kinematic and rheological model of exhumation of high pressure granulites in the Variscan orogenic root: example of the Blansky les granulite, Bohemian Massif, Czech Republic. Mineralogy and Petrology 86, 253–276.

Godard, G., van Roermund, H.L.M., 1995. Deformation-induced clinopyroxene fabrics from eclogites. Journal of Structural Geology 17, 1425–1443.

Heidelbach, F., Post, A., Tullis, J., 2000. Crystallographic preferred orientation in albite samples deformed experimentally by dislocation and solution precipitation creep. Journal of Structural Geology 22, 1649–1661.

Heilbronner, R., 2000. Optical orientation imaging. In: Jessel, M.W., Urai, J.L. (Eds.), Stress, Strain and Structure, A volume in honour of W.D. Means. Journal of the Virtual Explorer 2. http://virtualexplorer.com.au/VEjournal/Volume 2/.

Hippertt, J.F., 1994a. Microstructures and *c*-axis fabrics indicative of quartz dissolution in sheared quartzites and phyllonites. Tectonophysics 229, 141–163.

Hippertt, J.F., 1994b. Grain boundary microstructure in micaceous quartzite: significance for fluid movement and deformation processes in low metamorphic grade shear zones. The Journal of Geology 102, 331–348.

Ishii, K., Kanagawa, K., Shigematsu, N., Okudaira, T., 2007. High ductility of K-feldspar and development of granitic banded ultramylonite in the Ryoke metamorphic belt, SW Japan. Journal of structural Geology 29, 1083–1098.

Jessel, M.W., 1987. Grain-boundary migration microstructures in a naturally deformed quartzite. Journal of Structural Geology 9, 1007–1014.

Law, R.D., 1990. Crystallographic fabrics: a selective review of their applications to research in structural geology. In: Knipe, R.J., Rutter, E.H. (Eds.), Deformation Mechanisms, Rheology and Tectonics, 54. Geological Society of London, Special Publication, pp. 335–352.

Le Bayon, B., Pitra, P., Ballèvre, M., Bohn, M., 2006. Reconstructing P-T paths during continental collision using multi-stage garnet (Gran Paradiso nappe, Western Alps). Journal of Metamorphic Geology 24, 477–496.

Lister, G.S., 1977. Discussion: crossed-girdle c-axis fabrics in quartzites plastically deformed by plane strain and progressive simple shear. Tectonophysics 39, 51–54.

Mancktelow, N.S., 1979. The development of slaty cleavage, Fleurieu Peninsula, South Australia. Tectonophysics 58, 1–20.

Mancktelow, N.S., Pennacchioni, G., 2004. The influence of grain boundary fluids on the microstructure of quartz-feldspar mylonites. Journal of Structural Geology 26, 47–69.

Mancktelow, N.S., Grujic, D., Johnson, E.L., 1998. An SEM study of porosity and grain boundary microstructure in quartz mylonites, Simplon fault zone, Central Alps. Contributions to Mineralogy and Petrology 131, 71–85.

Martelat, J.-E., Schulmann, K., Lardeaux, J.-M., Nicollet, C., Cardon, H., 1999. Granulite microfabrics and deformation mechanisms in southern Madagascar. Journal of Structural Geology 21, 671–687.

Menegon, L., 2006. Ductile deformation of granitic rocks: selected examples from the Western Alps. Unpublished PhD Thesis, Università degli Studi di Padova, Italy.

Menegon, L., Pennacchioni, G., Stünitz, H., 2006. Nucleation and growth of myrmekite during ductile shear deformation in metagranites. Journal of Metamorphic Geology 24, 553–568.

Michibayashi, K., 1996. The role of intragranular fracturing on grain size reduction in feldspar during mylonitization. Journal of Structural Geology 18, 17–25.

Panozzo Heilbronner, R., Pauli, C., 1993. Integrated spatial and orientation analysis of quartz c-axes by computer-aided microscopy. Journal of Structural Geology 15, 369–382.

Passchier, C.W., Trouw, R.A.J., 1996. Microtectonics. Springer-Verlag, Heidelberg.

Prior, D.J., Trimby, P.W., Weber, U.D., Dingley, D.J., 1996. Orientation contrast imaging of microstructures in rocks using forescatter detectors in the scanning electron microscope. Mineralogical Magazine 60, 859–869.

Pryer, L.L., 1993. Microstructures in feldspars from a major crustal thrust zone: the Grenville Front, Ontario, Canada. Journal of Structural Geology 15, 21–36.

Pryer, L.L., Robin, P.-Y.F., 1996. Differential stress control on the growth and orientation of flame perthite: a paleostress-direction indicator. Journal of Structural Geology 18, 1151–1166.

Ring, U., Collins, A.S., Kassem, O.K., 2005. U-Pb SHRIMP data on the crystallization age of the Gran Paradiso augengneiss, Italian Western Alps: further evidence for Permian magmatic activity in the Alps during break-up of Pangea. Eclogae Geologicae Helvetiae 98, 363–370.

Rutter, E.H., 1976. The kinetics of rock deformation by pressure solution. Philosophical Transactions of the Royal Society of London A283, 203–219.

Sacerdoti, M., Labernardiere, H., Gandais, M., 1980. Transmission electron microscope (TEM) study of geologically deformed potassic feldspars. Bulletin de Minéralogie 103, 148–155.

Scandale, E., Gandais, M., Willaime, C., 1983. Transmission electron microscopic study of experimentally deformed K-feldspar single crystal. The (010) [001], (001) ½[110], (110) ½[112] and (111) ½[110] slip systems. Physics and Chemistry of Minerals 9, 182–187.

Schmid, S.M., Casey, M., 1986. Complete fabric analysis of some commonly observed quartz c-axis patterns. In: Hobbs, B.E., Heard, H.C. (Eds.), Mineral and Rock Deformations: Laboratory Studies. American Geophysical Union, Geophysical Monograph 36, 263–286.

Schulmann, K., Mlcoch, B., Melka, R., 1996. High-temperature microstructures and rheology of deformed granite, Erzgebirge, Bohemian Massif. Journal of Structural Geology 18, 719–733.

Simpson, C., Wintsch, R.P., 1989. Evidence for deformation induced K-feldspar replacement by myrmekite. Journal of Metamorphic Geology 7, 261–275.

Stallard, A., Shelley, D., 1995. Quartz *c*-axes parallel to stretching directions in very low-grade metamorphic rocks. Tectonophysics 249, 31–40.

Takeshita, T., Hara, I., 1998. *C*-Axis fabrics and microstructures in a recrystallized quartz vein deformed under fluid-rich greenschist conditions. Journal of Structural Geology 20, 417–431.

Tullis, J., 1983. Deformation of feldspars. In: Ribbe, P.H. (Ed.), Feldspar Mineralogy. Mineralogical Society of America, Reviews in Mineralogy 2, 297–323.

Tullis, J., Yund, R.A., 1977. Experimental deformation of dry Westerly granite. Journal of Geophysical Research 82, 5705–5718.

Tullis, J., Yund, R., Farver, J., 1996. Deformation-enhanced fluid distribution in feldspar aggregates and implications for ductile shear zones. Geology 24, 63–66.

Urai, J., Means, W.D., Lister, G.S., 1986. Dynamic recrystallization of minerals. In: Heard, H.C., Hobbs, B.E. (Eds.), Mineral and Rock Deformation: Laboratory Studies, the Paterson Volume. Geophysical Monograph, 36. American Geophysical Union, Washington DC, pp. 161–200.

Vernon, R.H., 2004. A Practical Guide to Rock Microstructure. Cambridge University Press, Cambridge.

Vernooij, M.G.C., den Brok, B., Kunze, K., 2006. Development of crystallographic preferred orientation by nucleation and growth of new grains in experimentally deformed quartz single crystals. Tectonophysics 427, 35–53.

Vidal, J.-L., Kubin, L., Debat, P., Soula, J.-C., 1980. Deformation and dynamic recrystallization of K-feldspar augen in orthogneiss from Montagne Noire, Occitania, Southern France. Lithos 13, 247–255.

Willaime, C., Christie, J.M., Kovacs, M.-P., 1979. Experimental deformation of K-feldspar single crystals. Bulletin de Minéralogie 102, 168–177.

Wintsch, R.P., Yi, K., 2002. Dissolution and replacement creep: a significant deformation mechanism in mid-crustal rocks. Journal of Structural Geology 24, 1179–1193.